

# A Robust SAR NLFM Waveform Selection Based on the Total Quality Assessment Techniques

I. Heidarpour Shahrezaei<sup>1</sup>, M. Kazerooni and M. Fallah

<sup>1</sup> Electrical Engineering Department, Malek Ashtar University of Technology, Tehran, IRAN

Corresponding author: kazerooni@mut.ac.ir

**Abstract-** Design, simulation and optimal selection of cosine-linear frequency modulation waveform (CNLFM) based on correlated ambiguity function (AF) method for the purpose of Synthetic Aperture Radar (SAR) is done in this article. The selected optimum CNLFM waveform in contribution with other waveforms are applied directly into a SAR image formation algorithm (IFA) and their quality effects performance in comparison to each other is analyzed. The quality performance analysis includes both the qualitative AF diagrams and the objective image quality metrics assessments. Then, by changing the SAR system parameters based on the proposed CNLFM waveform, other quality metrics are also derived. The simulation results verifies the robustness of the proposed CNLFM waveform implementation as a suitable NLFM alternative for LFM waveform.

**Index Terms-** Synthetic Aperture Radar, Non-Linear Frequency Modulation (NLFM), Ambiguity Function (AF), image formation algorithm (IFA), Waveform.

## I. INTRODUCTION

The synthetic aperture radar (SAR) technology is a major development of the modern active coherent microwave remote sensing technology. Compared with the optical system, SAR can not only achieve high resolution 2-D images, but also has the characteristics of all weather and all time with the application in the field of remote sensing, explorations, agriculture, military, etc.[1-3]. This coherent processing also known as the compression of frequency modulated pulse allows more energy to be transmitted and also better range resolution to be achieved[4]. SARs are available in different application modes which depends on the type of operation, target condition and image resolution[5]. Fig.1 shows a low squinted stripmap SAR with its simplified receiver model as one of the common types of airborne SARs with high imaging resolution. Due to its versatile applications, airborns with unusual flight characteristics can be equipped with this technique like missiles[6-9].

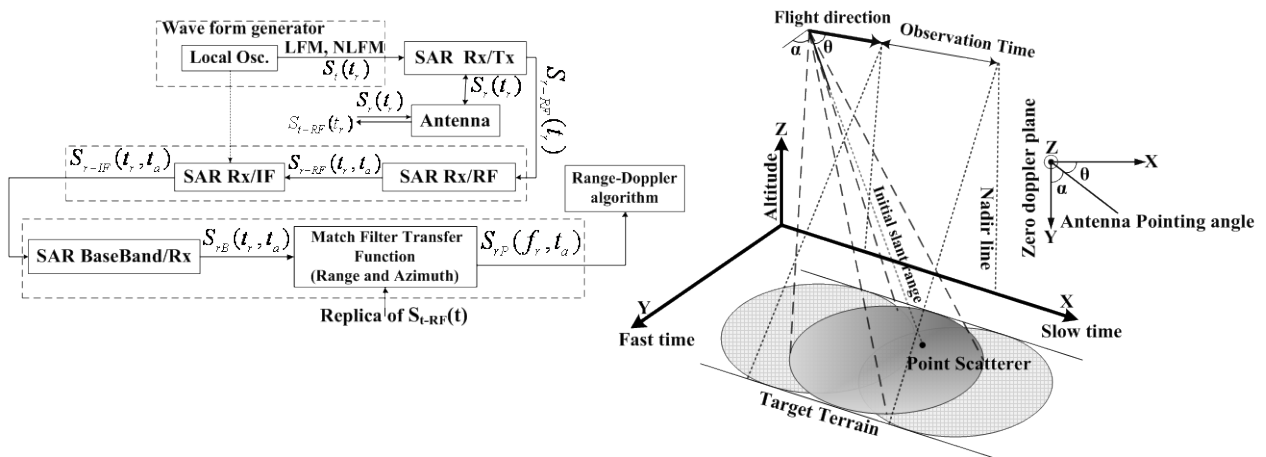


Fig. 1. The low squinted ( $\alpha=0$  to 6 Deg) missile-borne stripmap SAR flight geometry and receiver model

The most common type of pulse compression waveform is Linear Frequency Modulation (LFM) [6-9]. The match filter response of LFM has a side-lobe level of -13dB, which can be improved by some methods but at costs reducing SNR and wider mainlobe, which make it improper to use in SAR image formation [10]. Non-linear LFM (NLFM) is another pulse compression technique which can provide finer resolution, better SNR and good interference mitigation [5, 11-17]. It has a spectrum weighting function inherently in their modulation function, which could shape the power spectral density (PSD) of signal due to its instantaneous frequency as a non-linear function of time and result in a pure match filter giving low side-lobes [18]. The NLFM technique has been used such as discrete and continuous signal modulation [11-12]. Continuous NLFM waveforms with the help of phase modulation were devised in a way that provides very smaller sidelobe level, as well as the ability to be designed on hardware structures in contrast to discrete signal modulation [13-17]. In [13], the NLFM is designed based on piecewise linear functions as a method of instantaneous frequency function to generate the NLFM while no quality analysis is done for the NLFM. The radar ambiguity function (AF) as a complete quality assessment statement of the waveform provides an indication of the limitations and utility of different waveforms while assess the properties of the transmitted waveform regarding to their target resolution, measurement accuracy, ambiguity and responses to the backscattering [11, 14, 20]. In [13, 15-17], the NLFM is just used in an image formation algorithm (IFA) and no further AF quality analysis on the waveform design procedure is done. In this study, NLFM waveform design consideration based on AF quality analysis is firstly presented. Then, in comparison to [12-17] two different NLFM waveforms are not only simulated and evaluated based on AF quality analysis, but also were directly implemented to the SAR IFA for further quality assessment metrics extraction. The mentioned quality assessment techniques on the basis of the 2D image have not been done yet [11-17]. The qualitative AF analysis of the optimal SAR continuous NLFM waveform is done via ambiguity diagrams extraction [19], while the quantitative metric assessment is done via the calculation of mean square errors (MSE), signal-to-noise ratio (SNR), peak SNR (PSNR), PSD, normalized cross

correlation (NCC) and integrated side lobe ratio (ISLR) [20-21]. It should be noted that the effective antenna pointing angle on the basis of ISLR value is also extracted.

This paper is organized as follows. Firstly, both the LFM and the continuous NLFM waveforms are modeled based on correlated AF analysis. Section II, also introduces the proposed optimum continuous NLFM waveform selection based on AF quality analysis as well as the raw data generation. Section III, utilizes a range-Doppler algorithm (RDA) to generate the images of the proposed optimum cosine NLFM (CNLFM), while other images is derived. Section IV, contains complete quality metrics assessment techniques for evaluation of CNLFM waveform application in 2D SAR images while system parameters is being changed. Section V, presents conclusions on the simulation results and proposed topics for further researches.

## II. CONTINUOUS NLFM WAVE FORM QUALITY ANALYSIS BASED ON CORRELATED AF

On the basis of AF criterion of choice, this section includes the LFM and the NLFM waveforms simulations.

### A. LFM and NLFM waveform design considerations

The pulse compression method is the best technique to increase range resolution meanwhile SNR remains suitable in the receive process. The general form of LFM waveform is:

$$S_t(t) = A \cdot \text{rect}\left(\frac{t}{T}\right) \cos(2\pi f_0 t + \pi K_r t^2) \quad (1)$$

Where, T represents the radar pulse width,  $f_0$  is the carrier frequency,  $K_r$  is the chirp rate or the slope of the frequency alteration and  $A \cdot \text{rect}\left(\frac{t}{T}\right)$  is the signal amplitude modulation term, while the quadratic phase modulation presented as (2):

$$\varphi(t) = 2\pi f_0 t + \pi K_r t^2 \quad (2)$$

The LFM waveform spectrum with its chirp rate alteration is shown in Fig. 2. If the LFM waveform is designed in a way that its frequency alters asymmetrically within the bandwidth, the quadratic phase modulation will be changed as (3) which is called continuous NLFM:

$$\varphi(t) = \omega_0 t + K_r t^2 + \omega_n(t) \quad (3)$$

Where  $\omega_n(t)$  defines the non-linearity behavior of quadratic phase modulation of the waveform in shape of sine, cosine, tangent and etc. [22]. The designing of the NLFM waveform shapes the PSD to approach a required weighting function and cause the waveform does not have the SNR loss in contrast to LFM [11]. Fig.3 shows how the frequency alters with the time while the sine, the cosine and conventional linear functions are used. So, the NLFM has better detection rate characteristics than LFM and supposed to be more accurate in range determination for SAR application [23].

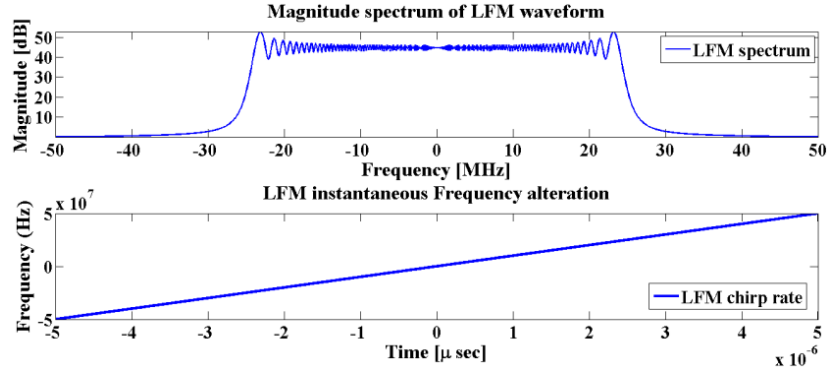


Fig. 2. SAR LFM waveform presentation [B=50MHz and T=10μsec and chirp rate=5×10<sup>12</sup>]

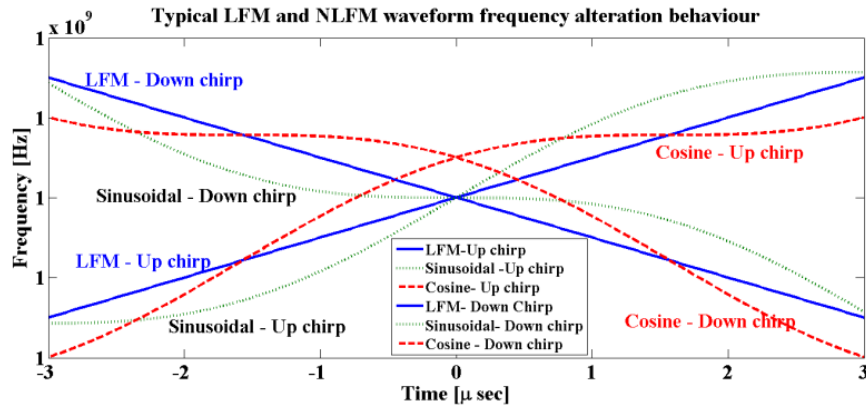


Fig. 3. Time-Frequency presentation of LFM and NLFM waveforms upchirp and downchirp state

The aim of the next section is to synthesize the LFM, continuous SNLFM and continuous CNLFM waveforms based on AF diagrams extraction.

### B. LFM and continuous NLFM qualitative analysis based on AF

Radar waveform AF is the output response of a single point scatterer at all possible combination of ranges and velocities. The AF of the SAR waveform can be defined in terms of cross-correlation of Doppler-shifted version of the transmitted waveform,  $S_t(t)$ , in the delay time and Doppler frequency plane,  $(\tau, f_d)$ , as Eq. (4):

$$|\chi(\tau; f_d)|^2 = \left| \int_{-\infty}^{+\infty} S_t(t) S_t^*(t - \tau) e^{j2\pi f_d t} dt \right|^2 \quad (4)$$

Where,  $\tau$  is the delay time and  $f_d$  is the Doppler frequency shift. According to Eq. (1) and Eq. (4), the AF of the LFM pulse can finally be written as Eq. (5):

$$|\chi(\tau; f_d)| = \left| \left(1 - \frac{\tau}{T}\right) \text{sinc}[\pi T(1 - \tau/T)(f_d + k_r \tau)] \right| \quad |\tau| \leq T \quad (5)$$

This relation represents both the LFM ambiguity diagram and the LFM ambiguity contour levels which are shown in Fig. 4. According to Eq. (1), Eq. (4) and Eq. (5) the LFM waveform AF diagrams are derived

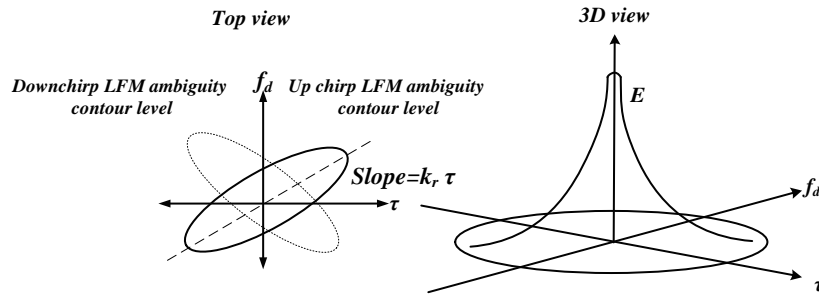


Fig. 4. 3D-view of ambiguity diagram and its pertinent ambiguity contour level

as Fig. 5. The same AF analysis including, ambiguity diagram, ambiguity contour levels, AF spectrogram and AF frequency profile for both of the continuous SNLFM and the continuous CNLFM are carried out, which are shown in Fig.6. It is deduced that different frequency chirp rates of the NLFM waveforms will lead to different ambiguity contour levels while presenting the similar ambiguity diagram is expected, because of similar inherent specifications of NLFM in comparison to LFM counterpart. The results are shown in Fig.5 (a), 5(b) and 6(a), 6(b).

According to Fig. 6 (c) , (d) and 6(e), (f) , the AF contour levels of CNLFM not only differs from the SNLFM but also is slightly more compact than LFM waveform which results in less spectral expansion of adjacent pixels and helps to improve the image quality. The NLFM waveform shapes the PSD to approach a required weighting function with lower sidelobes, while the CNLFM and SNLFM frequency profile has greater main-lobe level in comparison to LFM. On the other hand, CNLFM has distinctive lower side lobe level ratio in comparison to the SNLFM which makes it suitable for SAR image formation application. The results are clearly shown in Fig. 6(g), (h), (i), (j).

On the basis of AF diagram concepts, the requirements for ambiguity diagrams and exact resolution accuracy of SAR based on NLFM waveforms generation are not possible to achieve simultaneously. Hence, according to AF qualitative analysis, the continuous CNLFM with its compact contour levels and lower side-lobes is more proper for implementation than LFM and SNLFM.

### C. CNLFM Echo model analysis

According to flight geometry and SAR receiver model in Fig. 1, the received baseband echo signal of the point target in the distance fast time and azimuth slow time domain can be stated as Eq. (6):

$$s_r(t_r, t_a) = \exp \left\{ -j4\pi f_0 \frac{R(t_a)}{c} \right\} \exp \left\{ j\pi K_r \left( t_r - \frac{2R(t_a)}{c} \right)^2 \right\} \exp \left\{ j\pi \cos \left( t_r - \frac{2R(t_a)}{c} \right) \cdot \left( t_r - \frac{2R(t_a)}{c} \right) \right\} \quad (6)$$

Where,  $t_r$  is the range time,  $t_a$  is the azimuth time,  $s_r(t_r, t_a)$  is the received back scattered signal from the target,  $A$  is the received signal amplitude,  $w_r(\cdot)$  is the received pulse envelope,  $w_a(\cdot)$  is the transmitted pulse envelope in azimuth,  $f_0$  is the carrier frequency,  $K_r$  is the chirp rate and  $c$  is the speed of the light. The presented analysis is on the supposition that the platform stability is very high and is unaffected by the

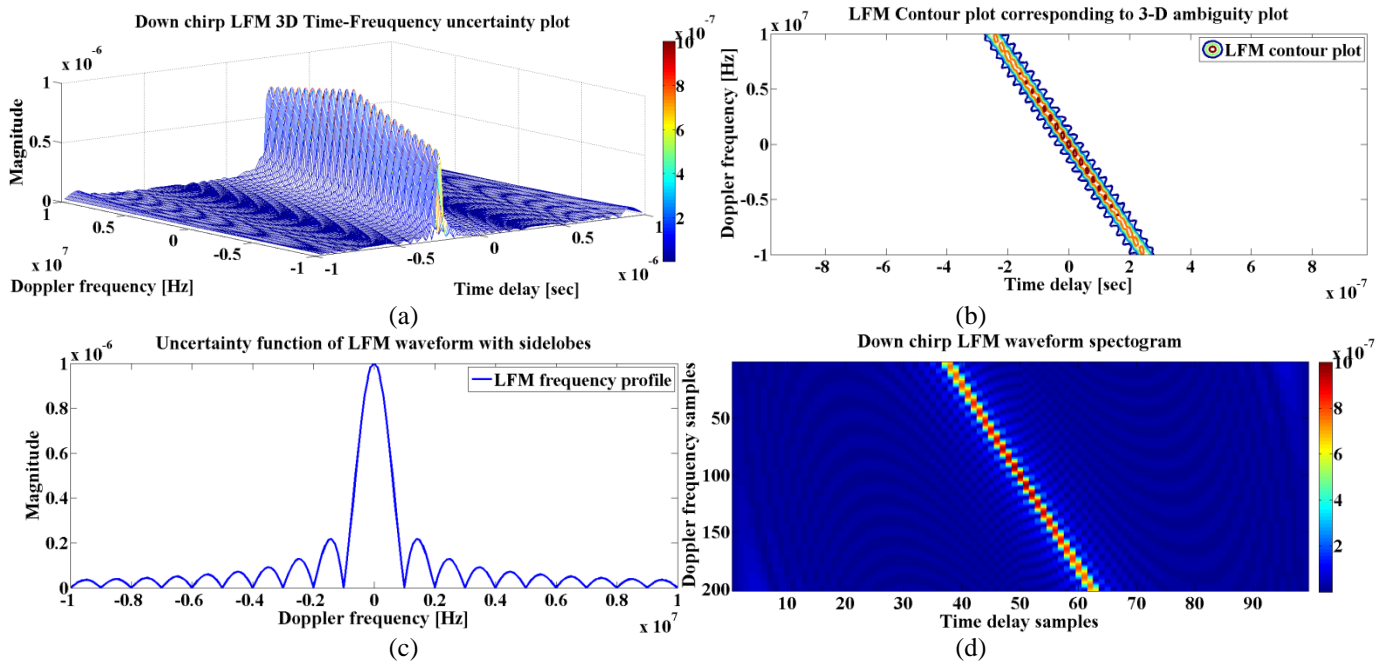
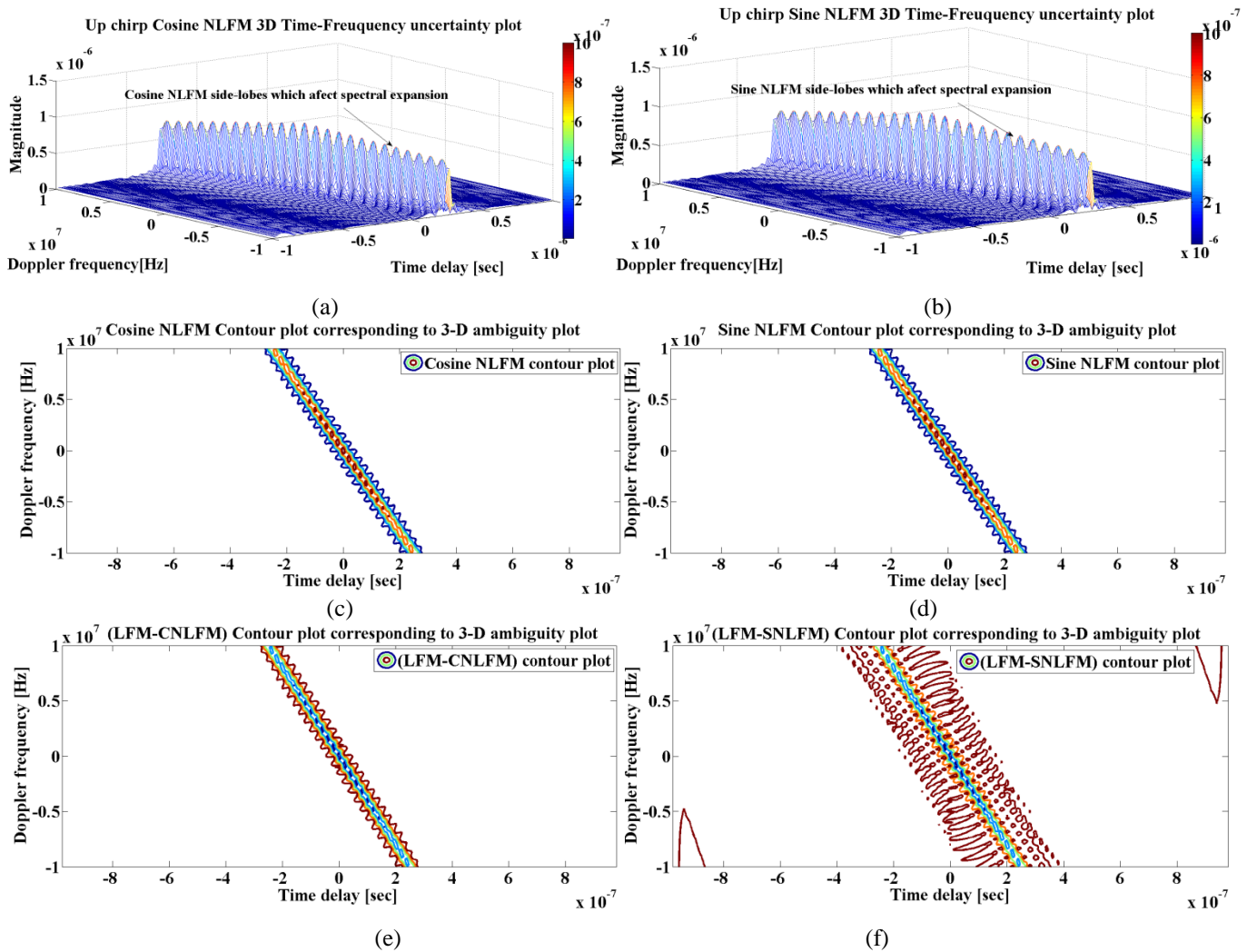


Fig. 5. LFM waveform AF simulation results (a) LFM waveform ambiguity diagram (b) LFM waveform ambiguity contour levels (c) LFM waveform AF frequency profile (d) LFM waveform AF spectrogram for (Pulse width=1  $\mu$ sec , Chirp rate= $4 \times 10^{13}$  down chirp)



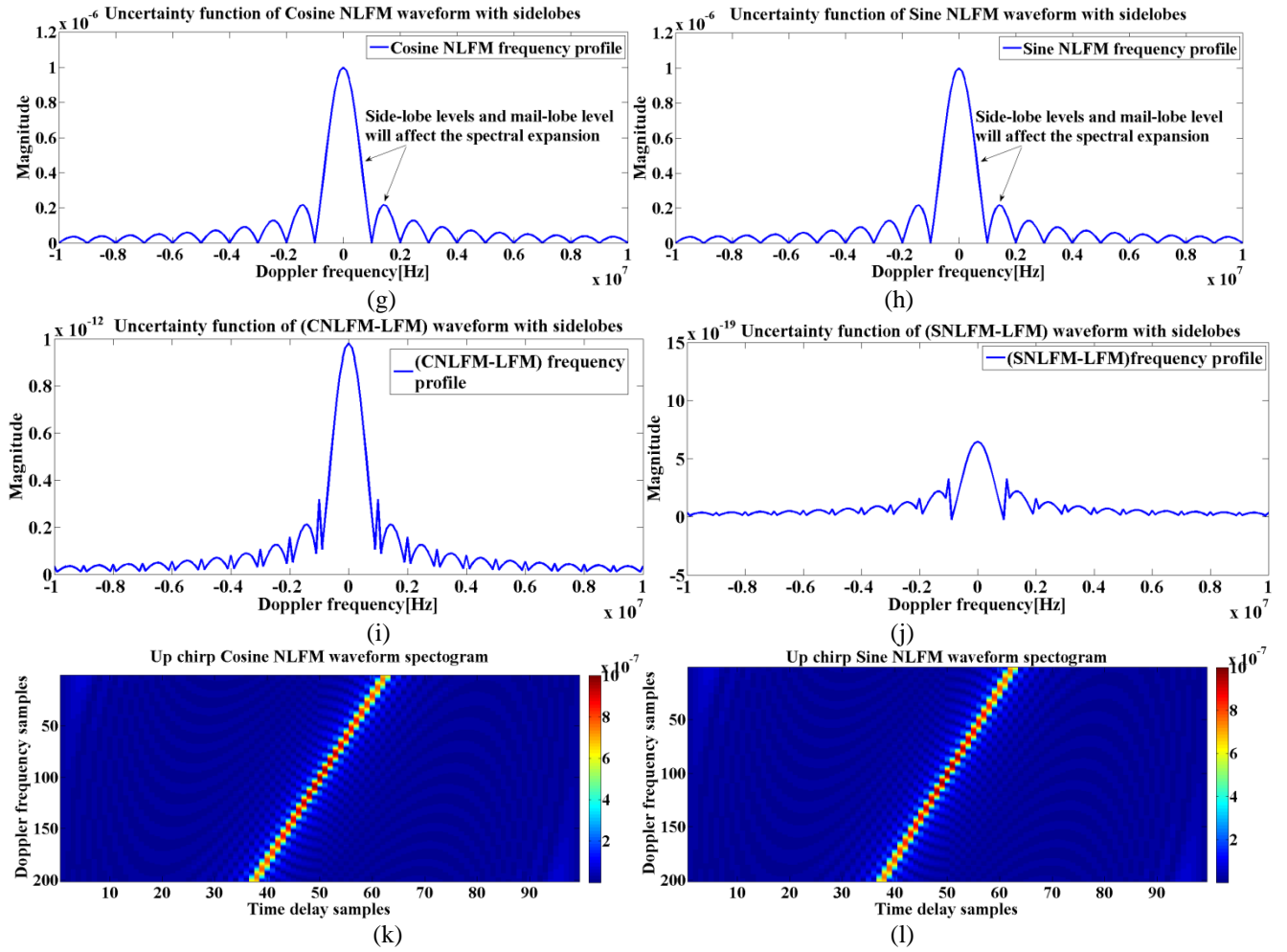


Fig. 6. NLFM wave forms AF simulation results (a) CNLFM waveform ambiguity diagram (b) SNLFM waveform ambiguity diagram (c) CNLFM waveform ambiguity contour levels (d) SNLFM waveform ambiguity contour levels (e) LFM- CNLFM waveform ambiguity contour levels (f) LFM- SNLFM waveform ambiguity contour levels (g) CNLFM waveform AF frequency profile (h) SNLFM waveform AF frequency profile (i) CNLFM –LFM AF frequency profile difference (j) SNLFM-LFM waveform AF frequency profile difference (k) CNLFM waveform AF spectrogram (l) SNLFM waveform AF spectrogram for (Pulse width = 1  $\mu$ sec , Chirp rate =  $4 \times 10^{13}$ )

radiometric motions. According to Fig. 1, in the case of straight flight path with broadside radiation, the slant range distance between the platform and a point target can be expressed as Eq. (7) [11]:

$$\begin{aligned}
 R(t_a) &= \sqrt{(x_i - vt_a)^2 + r_i^2} \\
 R(t_a) &= \sqrt{(R_0 \cos \alpha - vt_a)^2 + (R_0 \sin \alpha)^2} \\
 \alpha + \theta &= 90
 \end{aligned}
 \tag{7}$$

Where,  $v$  is the velocity of platform,  $R_0$  is slant range at the center of the aperture,  $\alpha$  is the squint angle measured between  $R_0$  and zero Doppler plane,  $\theta$  is the equivalent squint angle, and  $(x_i, r_i)$  is the point scatterer location over the target terrain. Hence, to investigate the performance of the proposed continuous CNLFM waveform, the SAR simulations are done based on system parameters in Table. I.

TABLE I. SAR SYSTEM PARAMETERS

Parameter	Value	Unit
Modulation type	CNLFM	-
Carrier frequency	15	GHz
Radar transmitter bandwidth	50	MHz
Chirp rate	$5 \times 10^{12}$	Hz/Sec
Pulse width	10	$\mu\text{sec}$
Azimuth sampling rate	2	KHz
Range sampling rate	60	KHz
Initial slant range	9452.2	Meter
Minimum slant range	9152	Meter
Maximum slant range	10947	Meter
Platform velocity	800	$m/\text{sec}$

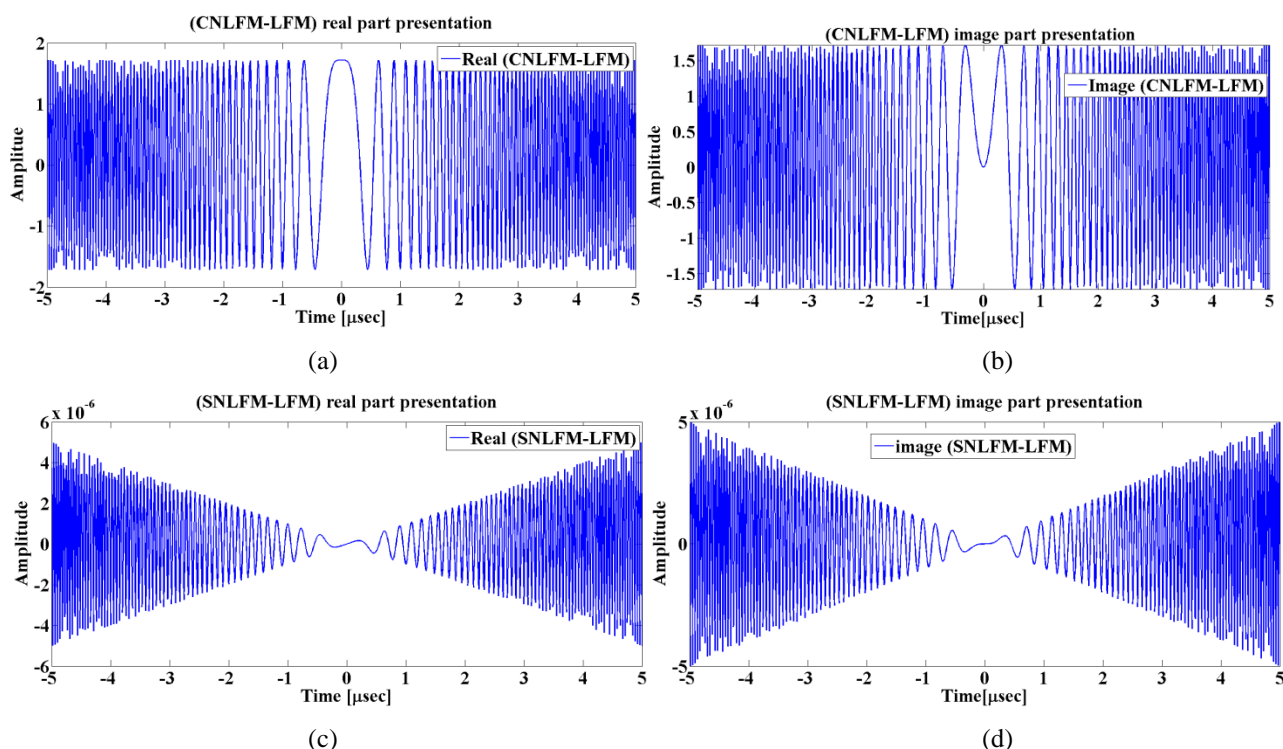


Fig. 7. NLFM difference with LFM (a) real (CNLFM-LFM) (b) image (CNLFM-LFM) (c) real (SNLFM-LFM) (d) images (SNLFM-LFM) for (Pulse width = 10  $\mu\text{sec}$ , Chirp rate =  $50 \times 10^{12}$  and Bandwidth 50MHz)

The magnitude differences of SAR chirp waveform for both of the continuous CNLFM and the continuous SNLFM with the LFM waveform on the basis of Table. I are shown in Fig.7. The non-linear inherent characteristics of NLFM modulation is the reason of differences in Fig. 7 (a) and 7(c) and 7(b), 7(d).

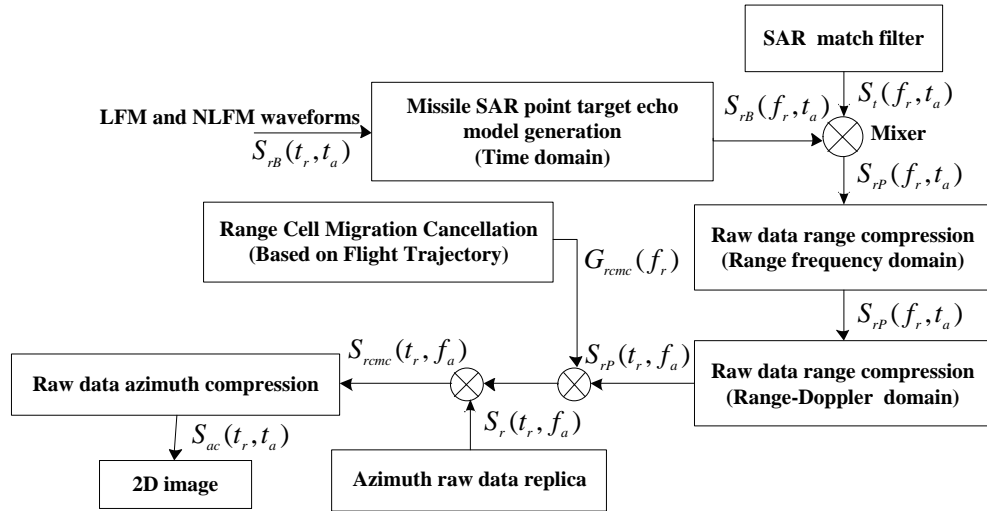


Fig. 8. RDA IFA for the proposed missile-borne SAR

### III. SAR IMAGE FORMATION ALGORITHM QUALITY ANALYSIS BASED ON NLFM WAVEFORMS

This section simulates the resulted images of received backscattered signal of single point target on the basis of LFM and NLFM waveforms with the help of RDA [11]. All the simulations are done based on the presumption of similar supersonic flight trajectory with the velocity of 800(m/sec). According to the flight geometry in Fig.1 and with the help of Eq. (6), the modified RDA processing procedure is proposed as Fig.8. It should be noted that the changes were made to the RDA because of different input waveforms.

#### A. Raw data generation

The RF input,  $s_{r-RF}(t_r, t_a)$ , firstly down converted into an intermediate frequency (IF) signal,  $s_{r-IF}(t_r, t_a)$ , and then directly transformed in to baseband,  $s_{rB}(t_r, t_a)$ , with the help of Eq. (6). Fig.1, Fig. 9(a) and 9(b) depict the non-linear characteristic of the frequency modulation in both the slow time and the fast time of the generated raw data,  $s_{rB}(t_r, t_a)$ , while continuous CNLFM and the SNLFM waveforms are being used.

#### B. Range compression

Range compression is performed with a fast convolution when the data are in the azimuth time domain  $(f_r, t_a)$ . In the other words, a range FFT is performed  $(f_r)$  on Eq. (6) followed by a range match filter multiply  $H(f_r)$ , and finally a range IFFT, to complete the range compression. This is done as equation (8):

$$s_{rc}(t_r, t_a) = \text{IFFT}_r\{s_r(f_r, t_a) \cdot H(f_r)\} = A \cdot P_r \left[ t_r - \frac{2R(t_a)}{c} \right] W_a(t_a - t_c) \exp \left\{ -j4\pi f_0 \frac{R(t_a)}{c} \right\} \quad (8)$$

Where,  $s_r(t_r, t_a)$  is the generated raw data,  $P_r(t_r)$  is the IFFT of the window  $w_r(f_r)$ ,  $s_r(f_r, t_a)$  is the range FFT of  $s_r(t_r, t_a)$ ,  $H(f_r)$  is the match filter function and  $s_{rc}(t_r, t_a)$  is the range compressed spectral

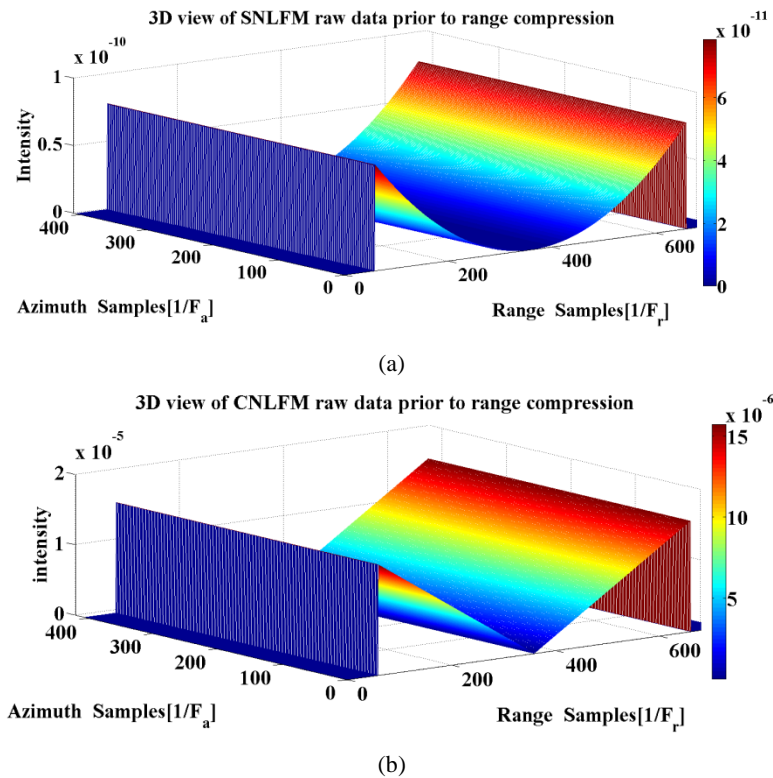


Fig. 9. 3D-view of Generated raw data (a) continuous SNLFM waveform (b) continuous CNLFM waveform

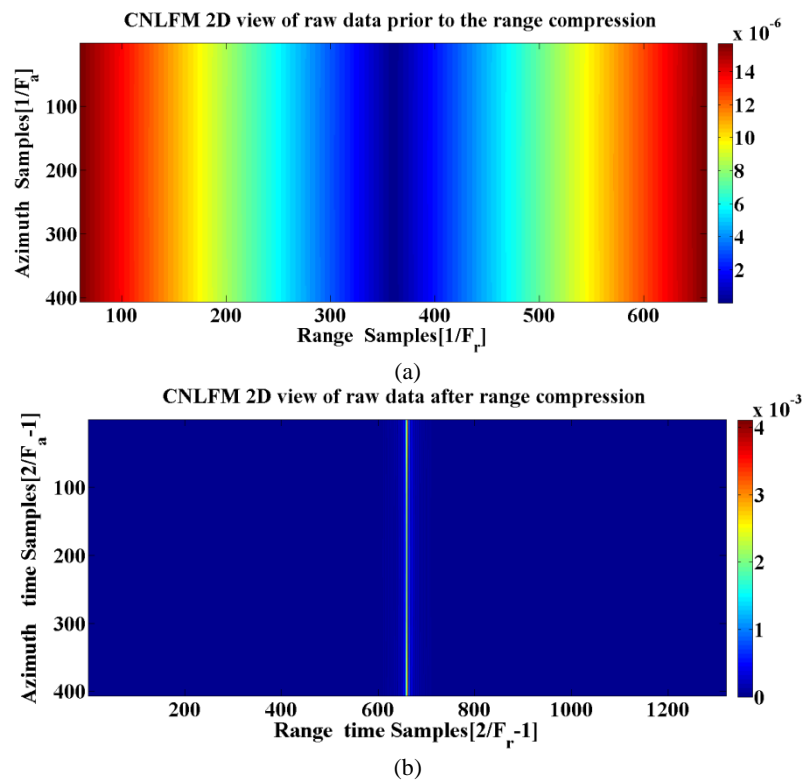


Fig. 10. 2D-view of CNLFM raw data (a) before range compression (b) after range compression

equation. For the simplicity the value of  $A$  is supposed to unit in order to compare the result of LFM, continuous CNLFM and SNLFM implementation in the final image. For a rectangular window or tapered

window,  $P_r(t_r)$  is sinc function or a sinc-like function with lower sidelobes. Fig. 10 (a) and (b) show both the CNLFM raw data and CNLFM raw data after range compression.

#### A. Azimuth FFT transform

An azimuth FFT transforms the data into the Range-Doppler domain  $(t_r, f_a)$  as Eq. (9):

$$S_1(t_r, f_a) = \text{FFT}_a\{S_{rc}(t_r, t_a)\} = A \cdot P_r \left[ t_r - \frac{2R(f_a)}{c} \right] W_a(f_a - f_c) \exp \left\{ -j4\pi f_0 \frac{R_0}{c} \right\} \exp \left\{ j\pi \frac{f_a^2}{K_a} \right\} \quad (9)$$

Where,  $S_1(t_r, f_a)$  is an azimuth FFT transform of range compressed data in the Doppler domain. The azimuth beam pattern  $w_a(t_a - t_c)$  is transformed into  $W_a(f_a - f_c)$ , with its shape preserved. The second phase term is the azimuth modulation which also has LFM and NLFM characteristic in  $f_a$ , while the first exponential term carries the inherent phase information of the target. The value of  $f_c$  is due to center frequency and center time,  $t_c$ .

#### B. Range Cell Migration Correction (RCMC)

RCMC is the range time and frequency dependent and it is performed in the Range-Doppler domain. The amount of RCM to correct is given by  $(\Delta R_{f_a})$  which is a function of azimuth frequency and represents the target displacement as a function of azimuth frequency. Note that  $\Delta R_{f_a}$  is also a function of  $R_0$  that is the range variant. The total procedure of RCMC is:

$$\begin{aligned} \Delta R_{f_a} &= \frac{\lambda^2 R_0 f_a^2}{8v_r^2} \\ G_{rcmc}(f_r) &= \exp \left\{ j \frac{4\pi f_r \Delta R_{f_a}}{c} \right\} \\ S_{rcmc}(t_r, f_a) &= S_2(t_r, f_a) \cdot G_{rcmc}(f_a) \\ S_2(t_r, t_a) &= \text{IFFT}_a\{S_{RCMC}(t_r, f_a)\} \end{aligned} \quad (10)$$

Where,  $\Delta R_{f_a}$  is the amount of RCM,  $G_{rcmc}(f_r)$  is the linear phase term of RCM,  $S_{RCMC}(t_r, f_a)$  is the corrected signal with RCMC and  $S_2(t_r, t_a)$  is the corrected signal in both range time and azimuth time.

#### C. Azimuth match filtering

Since the data after RCMC are in the Range-Doppler domain, it is convenient and efficient to implement the azimuth match filter in this domain as a function of slant range,  $R_0$ , and azimuth frequency,  $f_a$ . This step can be performed as the frequency domain match filter,  $H_a(f_a)$ , which is multiplied with the range gate as (11):

$$\begin{aligned} K_a &\approx \frac{2v_r^2}{\lambda R_0} \\ H_a(f_a) &= \exp \left\{ -j\pi \frac{f_a^2}{K_a} \right\} \\ S_3(t_r, f_a) &= S_2(t_r, f_a) \cdot H_a(f_a) = A \cdot P_r \left[ t_r - \frac{2R_0}{c} \right] W_a(f_a - f_c) \exp \left\{ -j4\pi f_0 \frac{R_0}{c} \right\} \end{aligned} \quad (11)$$

Where,  $H_a(f_a)$  is the frequency domain match filter,  $K_a$  is the function of  $R_0$ ,  $S_3(t_r, f_a)$  is the azimuth compression after RCMC.

#### D. Azimuth IFFT

This step, transforms the data back to the time domain, resulting in the complex image as Eq. (12):

$$S_{ac} = \text{IFFT}\{S_3(t_r, f_a)\} = A \cdot P_r \left[ t_r - \frac{2R_0}{c} \right] P_a(t_a) \exp \left\{ -j4\pi f_0 \frac{R_0}{c} \right\} \exp \{ j2\pi f_c t_a \} \quad (12)$$

Where,  $P_a(\cdot)$  is the amplitude of the azimuth impulse response, a sinc function similar to,  $P_r$ . The first exponential shows the target phase due to its range position,  $R_0$ , and the second is the linear phase term due to doppler center frequency. Accordingly, the final results of RDA using LFM, continuous SNLFM and the continuous CNLFM waveforms are shown in Fig.11 and Fig.12.

The  $f_a$  values and the  $f_r$  values in simulation results are azimuth and range sampling rate. According to spectral expansion simulation results in Fig. 11(b), 12(c) and 12(d) it is evident that waveform plays a key role in the pixel overlapping on the basis of non-linearity behavior of quadratic phase modulation which directly affects the reconstructed image. Similarly, the phase contour levels as shown in Fig. 11(c), 12(e) and 12(f) also have the same results while being analyzed on the basis of inherent non-linear modulation characteristics. The difference between Fig. 11(c), 12(e) and 12(f) is because of inherent differences of the AF contour levels which are existed in Fig. 5(b), 6(c) and 6(d). Likewise, frequency profiles are derived as Fig. 11(d), 12(g) and 12(h). It is obvious that Fig. 11(d) is quite different from 12(g) and 12(h), which is the result of the AF frequency profile in Fig. 5(c), 6(e) and 6(f). It should be noted that the reason of similarity between Fig. 12(g) and 12(h) is because of negligible difference in Fig. 5(c) and 6(e). Hence, the total procedure of the AF quality analysis of continuous NLFM waveforms shows that CNLFM waveform has more effects on the image contrast in comparison to the calculated frequency profile. On the other hand, in order to find the differences

between SNLFM and CNLFM, quantitative quality metrics would be a key which will be done on the RDA images in next section.

## IV. SAR RDA IMAGE FORMATION OBJECTIVE QUALITY ASSESSMENT EVALUATION

This section introduces and implements full-reference objective image quality assessment metrics on reference resulted LFM image and reconstructed NLFM images which are shown in Fig.11(a), 12(a), and 12(b).

### A. Objective NLFM waveforms image quality assessment metric definitions

The full-reference objective image quality metrics includes the SNR, PSNR, MSE, PSD, NCC and the ISLR. The SNR is calculated as the ratio of the mean value of the image and the standard deviation of the noise within the image. The higher the SNR value, the sharper the reconstructed NLFM images will be.

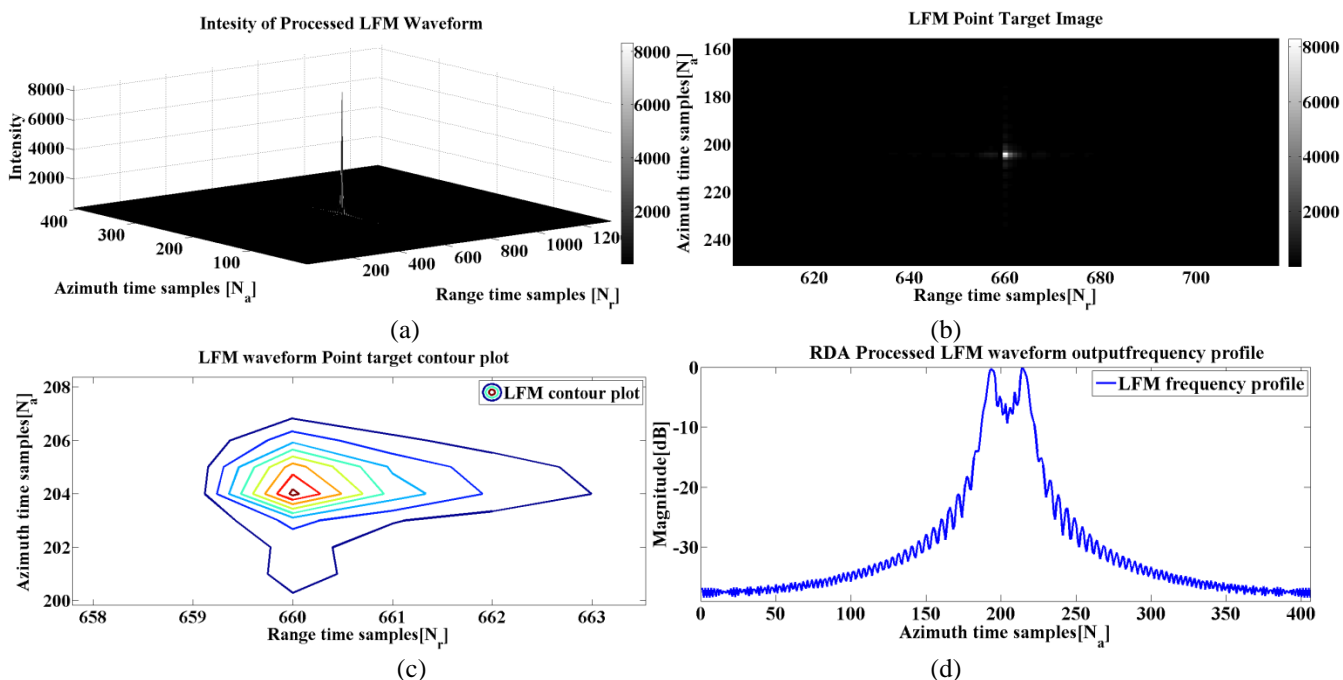


Fig. 11. final RDA image of single point scatterer with LFM waveform (a) 3D-view of RDA after azimuth compression (b) 2D-view of target spectral expansion (c) 2D-view of scatterer contour levels (d) received frequency profile of target

The PSNR is the ratio between the maximum possible power of the image and the power of corrupting noise that affects the quality of the image with the help of MSE as a scaled definition of power by the number of pixels in the images. There is an inverse relationship between PSNR and MSE. So, the higher the PSNR value indicates the higher quality of the reconstructed NLFM images which introduces the lower value of errors.

The PSD as a major quality assessment metric is also measures the strength of the energy as a function of frequency which shows at which frequencies variations are strong and at which frequencies variations are weak. The PSD is the best way to study the Non-linear modulation characteristics of the implemented NLFM waveforms in the SAR applications.

The NCC is used as a criterion to evaluate the degree of similarity between the LFM image as the reference waveform and the reconstructed CNLFM and SNLFM images which are proposed to replace the LFM. In addition to the qualitative comparison analysis based on the AF diagrams and aforementioned objective image quality metrics, ISLR is another important metric in SAR image quality assessment techniques. The ISLR measurement is done in a square area with 10 cells width and a center of maximum amplitude. It should be noted that, the simulations of continuous NLFM waveforms and LFM are carried out in the noise-free target terrain situation. However, the noisy condition does not affect the entity of the objective image quality assessment process on how the simulation is running, but the result values would

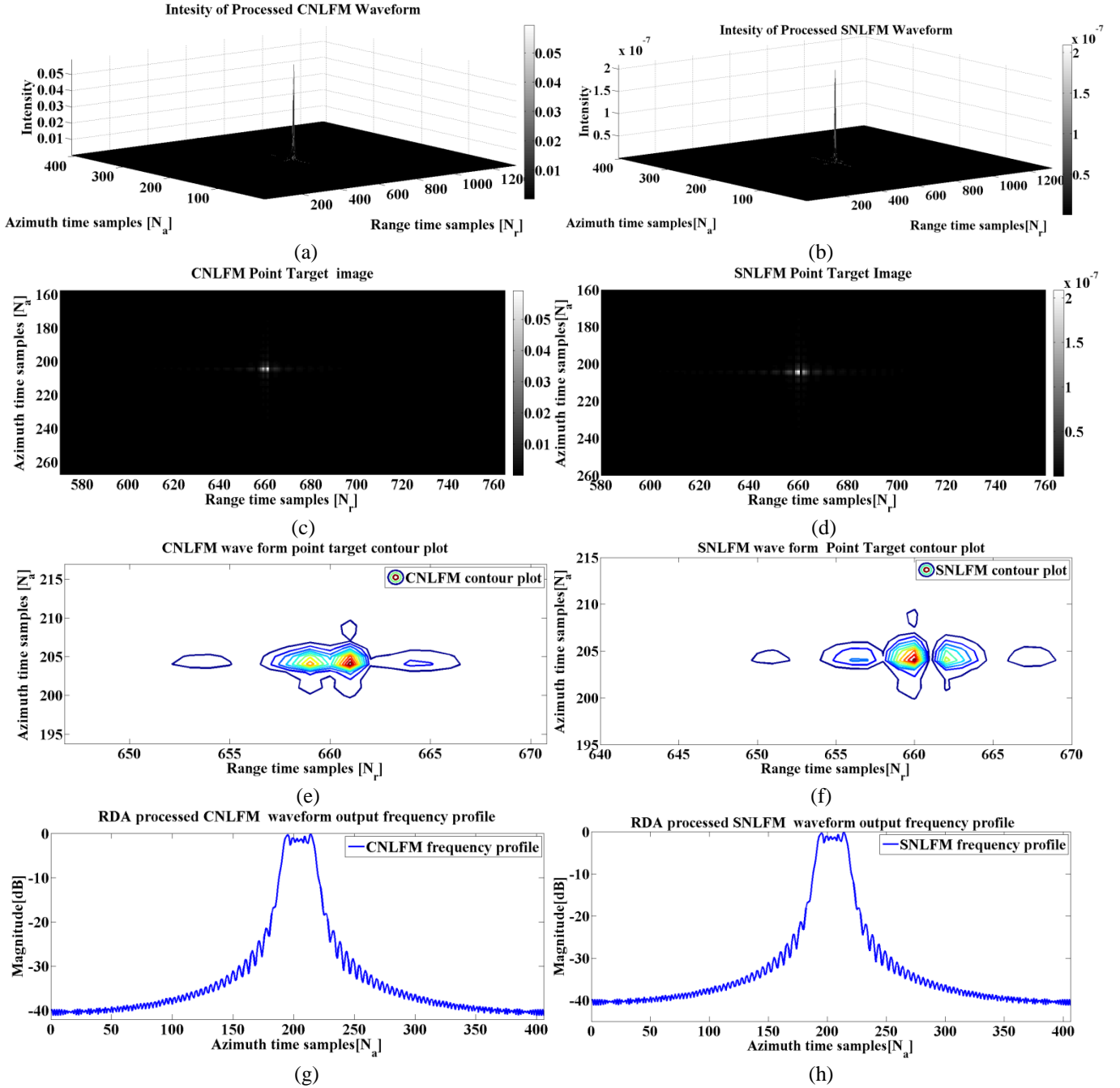


Fig. 12. (a) CNLFM 3D-view of RDA after azimuth compression (b) SNLFM 3D-view of RDA after azimuth compression (c) CNLFM 2D-view of target spectral expansion (d) SNLFM 2D-view of target spectral expansion (e) CNLFM 2D-view of scatterer contour levels (f) SNLFM 2D-view of scatterer contour levels (g) CNLFM received processed frequency profile (h) SNLFM received processed frequency profile

be different. In this paper it is basically focused on the NLFM waveforms applications and their effects on the quality while, the noisy channel is not opened.

### B. Objective NLFM waveforms image quality assessment simulation results

According to Section IV.A, the pixel difference-based measurements results are listed in Table.II, while, the input reference LFM image has an SNR of 52.14dB. On the other hand, about 0.8dB difference in the

SNR value between CNLFM and SNLFM confirms that CNLFM affects the image quality better than SNLFM. It should be noted that a noise free target terrain usually has SNR values higher than 50dB and the simulations verify the process of objective quality metrics extraction..

The PSNR calculation also illustrates that both the CNLFM and SNLFM waveforms have the same value because they are testing in noise-free situation and 23.008dB is acceptable. The MSE value is close to zero in such medium. The PSNR and MSE values are listed in Table.III.

In the case of dealing with the similar PSNR value for objective quality assessment, structural similarity index map (SSIM) is suitable alternative to demonstrate the performance of non-linear waveforms implementation in comparison to LFM. According to the presence of the single point scatterer, the SSIM difference of CNLFM and SNLFM reconstructed images is presented in Fig.13. As shown in Fig.13, it is deduced that the CNLFM image reconstruction is more efficient in comparison to the SNLFM. By applying 2D discrete Fourier transform on the reconstructed CNLFM and SNLFM images, their PSD is calculated. The PSD difference between the reference LFM image and the reconstructed CNLFM and SNLFM images, with the PSD difference between CNLFM and SNLFM images are also presented in Fig.14. Results in Fig.14, verifies that CNLFM has better PSD which means that energy distribution as a function of frequency are more efficient in comparison to SNLFM waveforms at the same frequencies. According to Fig.15, the NCC simulation results of CNLFM, SNLFM, an NCC difference about 0.4dB verifies that CNLFM has better effects in the image reconstruction based on cosine modulation. According to, Table. I and results in Fig .11(b) and Fig. 12(a), (b), the ISLR values for the LFM, continuous SNLFM and the continuous CNLFM are calculated as Table. IV. It shows that the ISLR value as an objective quality metric which is used specifically for SAR applications, verifies that the CNLFM has better performance in comparison to other waveforms. Besides the AF quality analysis and objective image quality assessment techniques, the impacts of SAR system parameters alteration on the ISLR while CNLFM is being used will be investigated here. Fig.16 shows the ISLR alteration while the SAR CNLFM transmitter bandwidth is being changed. It shows that the increase in in bandwidth up to 3 times will cause degradation of about 0.5dB in the ISLR value. Hence, the continuous CNLFM waveform is also robust to bandwidth alteration, which is the main parameter in SAR system resolutions. The antenna squint angle alteration is another concept in the analysis of SAR image objective image quality metrics based on ISLR value. Fig.17 shows that the increase in the antenna squint angle more than 6 degrees is not effective and for both the CNLFM waveform parameters an RDA must be modified to be adopted in the new squint angle. This alteration in the squint angle shows that a boundary of 6 degrees (from 0 to 6) is the effective antenna pointing angle while continuous CNLFM waveform is being used. It also shows that the ISLR is alternating between -10.46 dB to -16dB, which depicts 5dB robustness to the squint angle alteration. As

Table II. SNR value

Wave form	LFM	CNLFM	SNLFM
SNR [dB]	52.14	51.27	50.40

Table III. PSNR and MSE value

Wave form	PSNR	MSE
CNLFM	23.008 dB	0.01
SNLFM	23.008 dB	0.01

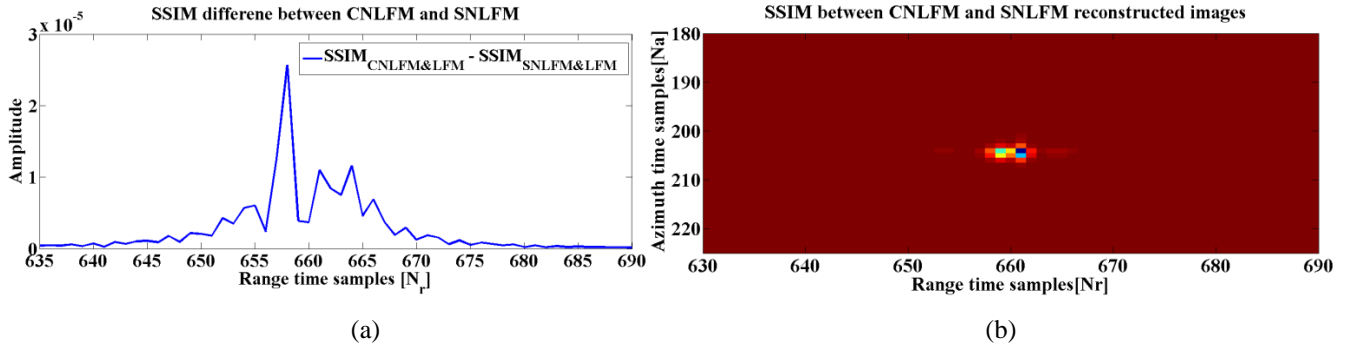


Fig. 13. SSIM difference of CNLFM and SNLFM (a) SSIM amplitude difference (b) 2D SSIM difference

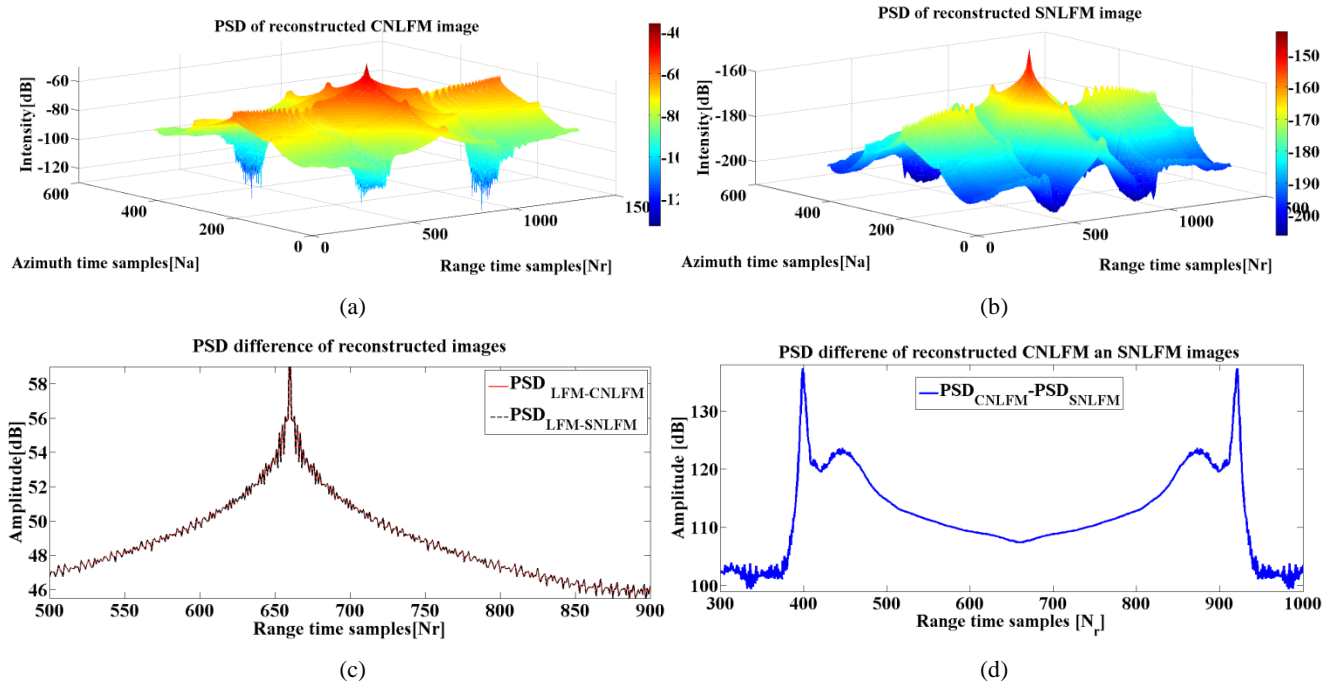


Fig. 14. PSD presentation (a) reconstructed CNLFM (b) reconstructed SNLFM (c) PSD difference between LFM , CNLFM and SNLFM (d) PSD difference between reconstructed CNLFM and SNLFM images

mentioned in Section.II, on the basis of AF contour levels, the NLFM waveforms affect the azimuth spectral expansion and weighing it. According to Fig.18, it is concluded that the CNLFM is no more robust against the squint alteration for  $\theta=14^\circ$ . So, not only the waveform systematic parameters must be changed, but also the RDA must be modified indeed. It should be noted that the increase in the squint angle while using linear or non-linear waveforms will always have a destructive effect on the ISLR value.

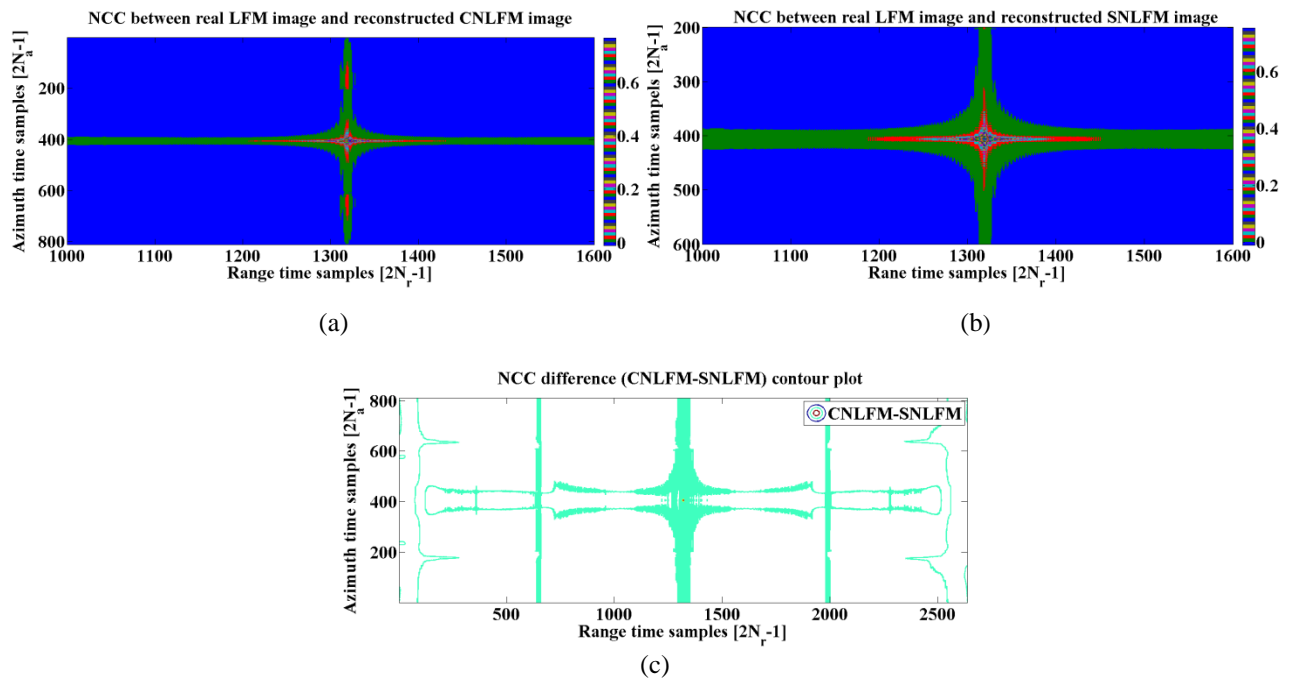


Fig. 15. NCC presentation (a) NCC of reconstructed CNLFM (b) NCC of reconstructed SNLFM (c) NCC difference contour between reconstructed CNLFM and SNLFM images

Table IV. Objective quality ISLR value

Wave form	ISLR
LFM	-10.395 dB
CNLFM	-10.467 dB
SNLFM	-10.272 dB

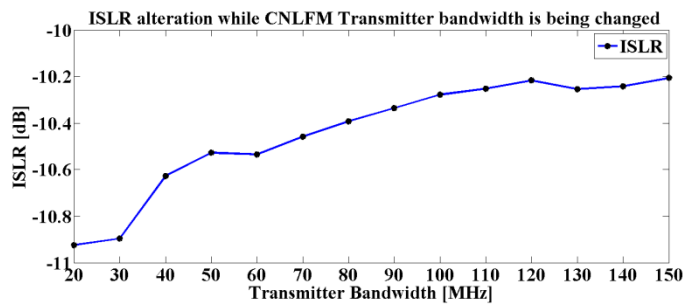


Fig. 16. ISLR alteration while radar transmitter bandwidth is being changed

The ISLR sensitivity to the center frequency alteration while other system parameters remain unchanged is also shown in Fig.19. It shows the irregular deviation in the ISLR value when the center frequency alters. More precisely, the impact of this deviation in the image quality index can be investigated in equations (10), (11), (12) and image formation design procedures. In other words, the main steps of the IFA is directly depending on the center frequency and sampling rates. On the other hand, the flight geometry and radar system parameters mutually depending together, in which modifying one of them must be accompanied with the correction of the other one. Otherwise, the system will not respond correctly. So,

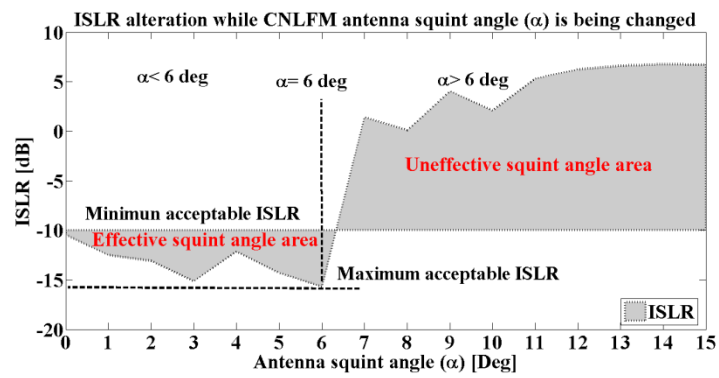


Fig. 17. Proposed CNLFM waveform image, ISLR alteration while antenna squint angle is being changed

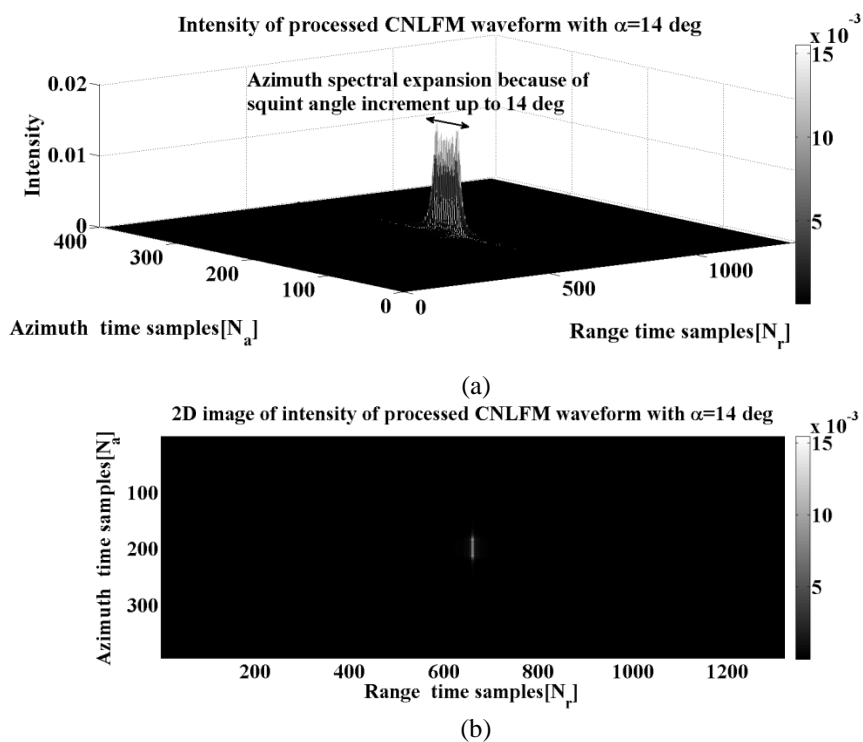


Fig. 18. Proposed CNLFM spectral expansion while squint angle increased up to 14deg (a) 3D-view (b) 2D-view

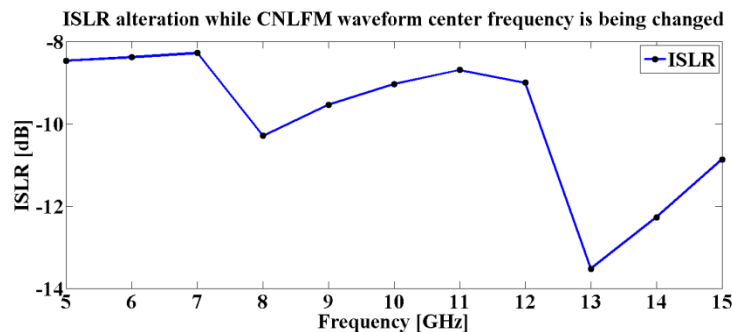


Fig. 19. ISLR alteration while center frequency is being changed based on proposed CNLFM waveform

changing the center frequency without correcting the other system parameters and IFA steps will lead to such response.

Table.V. SAR system parameters qualitative effect on the image and ISLR value

Type of change	Total effects
Squint angle deviation	Direct effects on the ISLR value
Transmitter bandwidth	Direct effects on the range resolution
Synthetic aperture observation time	Direct effects on the azimuth resolution

Hence, the continuous CNLFM waveform performance in comparison to the continuous SNLFM is discovered more robust and introduces itself as a robust alternative to LFM counterpart. Table.V. summarizes the results of the SAR system parameters alteration in the ISLR index qualitatively.

## V. CONCLUSION

This article compares the characteristics of LFM, continuous SNLFM and continuous CNLFM waveforms based on their AF quality analysis and subsequently, the optimum continuous CNLFM waveform is selected for further analysis. The impact of CNLFM implementation was investigated in comparison to LFM and SNLFM with the help of objective image quality assessment metrics analysis. All the simulations were carried out based on the similar flight trajectory and system parameters. On the other hand, complete objective image quality assessment metrics were derived and compared to each other. The SNR, PSNR, MSE, PSD, NCC and ISLR value were extracted and compared based on using different waveforms. All the results validate that CNLFM waveform is not only a suitable alternative for LFM but also is more robust than SNLFM and even some cases to LFM. As verified above, the PSD of CNLFM in comparison to SNLFM and LFM make it more suitable for using in electronic warfare environments.

The ISLR comparison results show that the continuous CNLFM waveform not only reduces the level of the side-lobes but also it increases the main-lobe level up to 1.2 times and makes the IFA more robust against spectral expansion and Doppler deviations in the image. The continuous CNLFM waveform robustness procedure is evaluated by changing the antenna squint angle and bandwidth while the ISLR value of the image is measured. The results presented in tables, indicate that the increase in bandwidth up to 3 times will have a degradation of 0.5 dB in the ISLR, while increasing the squint angle up to 6 degrees will reduce the ISLR value about 5dB.

Future activities in the context of this article might involve using new the waveforms, increasing the squint angle and modifying the image formation algorithm, using the method of time-frequency processing in the IFA processing.

## REFERENCES

- [1] J. J. Kovaly, *Synthetic Aperture Radar*, Artech House, Dedham, MA, 1976.
- [2] G. Franceschetti, M. Migliaccio, and D. Riccio, "SAR simulation of actual ground sites described in terms of sparse input data," *IEEE Trans. Geoscience and Remote Sensing*, vol. 32, no. 6, pp. 1160–1169, Nov. 1994.

- [3] M. I. Skolnik, Introduction to Radar Systems, McGraw-Hill, New York, 2001.
- [4] M. Sack, M. R. Ito and I. G. Cumming, "Application of efficient linear fm matched filtering algorithms to synthetic aperture radar processing," IEE Proceedings, vol. 132, pp. 45-57, Feb. 1985.
- [5] R. Sullivan, *Synthetic Aperture Radar*, in M. I. Skolnik *Radar Handbook*, 3<sup>rd</sup> Ed, New York: McGraw Hill, 2008.
- [6] J. Zhu, Zh. He, Bo. Zhou and J. Li, "real-time signal processing implementation of the missile-borne sar using high performance DSP," IEEE, Int. Conference on Radar, pp. 1-4, Oct. 2006.
- [7] Y. Liu, M. Xing, G. Sun, X. Lv, Z. Bao and W. Hong, "Echo model analysis and imaging algorithm for high-resolution SAR on high-speed platform," IEEE Trans. on Geoscience and Remote Sensing, vol.50, no.3, pp. 933-950, Sept. 2012.
- [8] Y. Yusheng, Zh. Linrang, L. Yan, L. Nan and L. Xin, "Range Doppler algorithm for bistatic missile-borne forward-looking SAR," IEEE second APSAR, pp. 960-963, Oct. 2009.
- [9] Zh. Yingxi, L. Ming, "A design of motion compensation for high resolution imaging of missile-borne SAR," IEEE ICCAS, pp. 427-430, Sept. 2009.
- [10] E. De Witte and H. D. Griffiths, "Improved ultra-low range side-lobe pulse compression waveform design," IEEE Electronics Letters, vol. 40, no. 22, pp. 1448-1450, Nov. 2004.
- [11] S. F. Li, J. Chen, L.Q. Zhang and Y.Q. Zhou, "Image formation algorithm for missile-borne MMW SAR with phase coded waveform," IET Int. Conference on Radar, pp. 1-4, Dec. 2009.
- [12] James M. Kurdzo, Boon Leng Cheong, Robert D. Palmer, Guifu Zhang, "Optimized NLFM pulse compression waveforms for high-sensitivity radar observations," Int. Radar Conference (Radar), pp.1-6 ,Oct. 2014.
- [13] J. Saeedi and K. Faez, "Synthetic aperture radar imaging using nonlinear frequency modulation signal," IEEE Trans. on Aerospace and Electronic Systems ,vol. 52, issue. 1, pp. 99-110, Feb. 2016.
- [14] S. Boukeffa, Y. Jiang, T. Jiang, "Sidelobe reduction with nonlinear frequency modulated waveforms," IEEE 7th Int. Colloquium on Signal Processing and its Applications (CSPA), pp. 399-403, May 2011.
- [15] M. Luszczuk, "Numerical evaluation of ambiguity function for stepped non-linear FM radar waveform," International Conference on Microwaves, Radar & Wireless Communications (MIKON), pp.1164 – 1167, May 2006.
- [16] W. Wang, R. Wang, Y. Deng, Z. Zhang, X. Wu, and Z. Xu, "Demonstration of NLFM waveforms with experiments and doppler shift compensation for SAR Application," IEEE Geoscience and Remote Sensing Letters, vol. 13, issue 12, pp. 1999-2003 , Dec. 2016.
- [17] W. Wang, R. Wang, Z. Zhang, Y. Deng, N. Li, L. Hou, and Z. Xu, "First demonstration of airborne SAR with nonlinear FM chirp waveforms," IEEE Geoscience and Remote Sensing Letters, vol. 13, no. 2, pp. 247-251, Feb. 2016.
- [18] Y. K. Chan, M. Y. Chua, and V. C. Koo, "Side-lobes reduction using simple two and tri-stages non-linear frequency modulation (NLFM)," Prog. Electromagn. Res., vol. 98, pp. 33-52, 2009.
- [19] B. R. Mahafza., *MATLAB Simulations for Radar System Design*, Chapman & Hall, 2004.
- [20] X. Lu and H. Sun, "Parameter assessment for SAR image quality evaluation system" in Proc. 1<sup>st</sup> APSAR, pp. 58-60, Nov. 2007.
- [21] I. Heidarpor, M. Kazerooni, M. Fallah, "A complex target terrain SAR raw data generation and evaluation based on inversed equalized hybrid-domain algorithm processing," Waves in Random and Complex Media (WRCM), vol.27, issue 1, pp. 47-66, Jan. 2017.
- [22] W. G. Carrara, R. S. Goodman, and R. M. Majewski, *Spotlight Synthetic Aperture Radar: Signal Processing Algorithms*, Norwood, MA, USA: Artech House, 1995.
- [23] F. J. Harris, "On the use of windows for harmonic analysis with the discrete Fourier transform", Proceedings of the IEEE, vol. 66, pp. 51-84, Jan. 1978.